Gas phase dehydration of C_6 alcohols promoted by Y zeolite and supported nafion catalysts

Colin Park [a], Mark A. Keane [a,b,*]

[a] *Department of Chemical Engineering, University of Leeds, Leeds LS2 9JT, UK*
[b] *Deparment of Chemical and Materials Engineering, University of Kentucky, Lexington, KY 40506-0046, USA*

Abstract

The gas phase dehydration of hexan-1-ol, hexan-2-ol and cyclohexanol ($473 \, K \leq T \leq 573 \, K$) has been studied over NaY, HY and Ni/NaY zeolites and the action of each has been compared with a commercially available 13% w/w Nafion/SiO$_2$ composite. The Ni exchanged zeolite and Nafion catalysts exhibited a high selectivity in terms of alkene formation. Condensation to generate the respective ether represented a secondary process that was not promoted to the same extent. Reaction over the Nafion sample was characterised by an initial increase in conversion with time that can be linked to a gradual swelling of the polymeric matrix by water produced in the dehydration step. Reduction of the Ni/NaY zeolites in flowing hydrogen generated surface Brønsted acidity that has been characterised by IR, NH$_3$ chemisorption and iodometric titration. Dehydration activity in the case of NaY and Ni/NaY was directly proportional to acid site concentration and there was little dependence on acid site strength. The effect of reaction time, temperature and gas space velocity on activity/selectivity is presented and discussed. Catalysis over the zeolites was accompanied by appreciable deactivation due to coke formation that was also dependent on surface acid site concentration. A high carbon (up to 50% w/w) content was recorded for the spent zeolites but the presence of nickel metal served to limit the deposition of highly amorphous carbonaceous species. The applicability of a reductive regeneration of the used zeolites is considered. Carbon monoxide chemisorption/desorption and TEM/SEM analysis have revealed weak interaction(s) between the Ni crystallites and the aluminosilicate support. An appreciable growth of the supported nickel particles during catalysis was detected and is quantified. © 2001 Elsevier Science B.V. All rights reserved.

Keywords: Zeolite Y; Acid catalysis; Brønsted acidity; Alcohol dehydration; Nafion composite; Catalyst deactivation; Nickel exchanged zeolite

1. Introduction

The catalytic dehydration of alcohols to the respective ethers and/or alkenes is assuming increasing importance as a synthetic methodology. The direct dehydration of an alcohol to an alkene is problematic in that highly acidic reaction conditions are required [1] and the alkene that is generated in such an environment is susceptible to further reaction. In order to circumvent this eventuality, the alcohol is generally reacted as a halide or in a sulphonated form [2–4]. A less aggressive and more direct "alcohol to alkene" route would certainly fill a commercial need. Ethers, as the alternative products are also highly desirable commodities as oxygenate fuel additives [5,6]. The dehydration of alcohols, both in the gas and liquid phase, has been promoted using a variety of catalysts [7–9] and a number of contrasting mechanisms have been proposed [10–19] to link catalytic activity to the nature of the alcohol/catalyst reaction system. The

* Corresponding author. Tel.: +1 859-257-8028;
fax: +1 859-323-1929.
E-mail address: makeane@ergr.uky.edu (M.A. Keane).

reaction can proceed in the absence of a catalyst as demonstrated by Chénedé et al. [1] but a catalytic route that offers high selectivity to the desired product(s) is a far more cost effective approach.

The dehydration of alcohols and the reverse (hydration) reaction have been used to assess catalytic acidity in both homogeneous and heterogeneous systems [5,9,20–22]. A loss of activity has been ascribed to a poisoning by both the product (water) [23] and alcohol reactant [24]. Ballantine et al. [25] studied the liquid phase dehydration of alcohols (at 473 K) over montmorillonite catalysts and concluded that primary alcohols underwent preferential intermolecular dehydration to cede dialkyl ethers in high yields while secondary alcohols favoured the formation of the alkene via a facile intramolecular dehydration pathway. The conversion of both methanol and ethanol [26,27] over alumina yielded the dialkyl ether (and water) as the major product(s) where an increase in reaction temperature induced alkene formation. The consensus of opinion is that, over solid catalysts, lower reaction temperatures favour the formation of the ether while the alkene is preferred at higher temperatures [5,22].

Solid acid catalysts that have found use in dehydration and related processes include sulphonated ion exchange polymeric resins [2–4,28], sulphonated zirconia [29] and zirconium phosphate [30]. Nafion is a perfluorinated sulphonic acid resin, characterised as a highly acidic medium but with the limitation of having a low surface area [4,5,31,32]. In order to utilise the inherent high acidity of Nafion, the polymer can be dispersed on an amorphous silica matrix. Heidekum et al. [33,34] have recorded high activities and selectivities in the (demanding) acylation of aromatics over a 13% w/w Nafion/SiO$_2$ (SAC-13) composite. The application of zeolitic materials, such as H-ZSM-5 [17,35,36] and X and Y faujasites [18,20,21] in both the protonated and indigenous alkali forms has also been reported. Alcohol dehydration over transition metal exchanged zeolites has, by comparison, received scant attention in the literature. The balance between acidic and basic functions in alkali exchanged zeolites is known to have a significant impact in organic rearrangement reactions [34,37,38]. We examine, here, the interplay between zeolitic metal and acid sites in controlling catalytic dehydration and consider the possible contribution that the steric restrictions imposed by the uniform microporous structure can play.

As a model system, we have studied the influence of Ni loading on the catalytic action of Ni/NaY in the gas phase dehydration of C$_6$ straight, branched and cyclic alcohols. The action of a fully protonated HY zeolite and a commercially available Nafion/SiO$_2$ composite have also been assessed for comparative purposes. The effect of varying such process variables as reaction temperature and contact time is considered, catalyst deactivation and regeneration are addressed while a comprehensive programme of catalyst characterisation, before and after reaction, has been conducted in an attempt to link the observed activities/selectivities to the nature of the surface acid and metal sites.

2. Experimental

2.1. Catalyst preparation and activation

The zeolite catalysts were prepared by ion exchange of a Linde LZ-52Y aluminosilicate that has the unit cell composition given in Table 1. In order to obtain, as far as possible, the homoionic sodium form the zeolite as received was contacted five times with 1 mol dm^{-3} NaNO$_3$ solutions. The Ni/NaY samples were prepared by exchanging 20 g of the parent NaY with 200 cm^3 of 0.1 mol dm^{-3} Ni(NO$_3$)$_2$ at 373 ± 2 K where the suspension was kept under constant agitation (600 rpm). The system was allowed to equilibrate for 48 h at which point the zeolite was separated by filtration, washed with hot deionised water (3 × 50 cm^3), oven-dried at 363 K for 24 h and stored over saturated NH$_4$Cl at room temperature. The Ni and Na contents were determined (to within ±2%) by atomic absorption spectrophotometry (VarianSpectra AA-10). Higher Ni loadings were achieved by repeated exchange and the unit cell compositions of the three Ni exchanged zeolite samples employed in this study are given in Table 1. It can be seen that Ni exchange was accompanied by a minor degree of decationation as a result of hydronium ion exchange. The exchange procedure is described in much greater detail elsewhere [39–41]. The hydrated zeolite catalyst precursors, sieved in the 200–150 μm range were activated by heating at 10 K min^{-1} in 100 cm^3 min^{-1} dry 20% v/v H$_2$/He to 723 K, maintaining this temperature for 16 h. The ammonium form was prepared by repeatedly refluxing 20 g of the parent NaY with 200 cm^3 0.5 mol dm^{-3} NH$_4$NO$_3$ solutions as above; the acti-

Table 1
Unit cell composition of the parent NaY zeolite, the protonic form and the three Ni exchanged samples

Sample	Unit cell composition	Ni w/w (%) (hydrated)	Ni w/w (%) (dehydrated)
NaY	$Na_{58}^+ (AlO_2)_{58}^- (SiO_2)_{134} \cdot xH_2O$	–	–
HY	$H_{58}^+ (AlO_2)_{58}^- (SiO_2)_{134} \cdot xH_2O$	–	–
Ni/NaY-A	$Ni_{5.0}^{2+} H_{0.5}^+ Na_{47.5}^+ (AlO_2)_{58}^- (SiO_2)_{134} \cdot xH_2O$	1.9	2.5
Ni/NaY-B	$Ni_{10.4}^{2+} H_{1.2}^+ Na_{36.0}^+ (AlO_2)_{58}^- (SiO_2)_{134} \cdot xH_2O$	3.4	4.7
Ni/NaY-C	$Ni_{14.1}^{2+} H_{1.0}^+ Na_{28.8}^+ (AlO_2)_{58}^- (SiO_2)_{134} \cdot xH_2O$	6.4	8.9

vated protonic form is given in Table 1. The activated catalysts were cooled to reaction temperature in the H_2/He mixture and the system thoroughly flushed in dry He ($100 \, cm^3 \, min^{-1}$ for 1 h) before the alcohol reactant was introduced. A 13% w/w Nafion/SiO$_2$ (SAC-13) composite, supplied by Dupont Fluoro-products was activated by heating at $5 \, K \, min^{-1}$ in $100 \, cm^3 \, min^{-1}$ dry He to 413 K which was held for 4 h before reverting to the reaction temperature.

2.2. Catalyst characterisation

The water content of the hydrated catalyst precursors was measured by thermogravimetric/differential scanning calorimetry (TG/DSC); the samples were ramped ($5 \, K \, min^{-1}$) to 873 K in dry N_2. The degree of Ni^{2+} reduction was determined by iodometric titration as described in detail elsewhere [39] and the surface Brønsted acidity was assessed by infra-red analysis [40]. Surface acidity was also probed by NH_3 adsorption at 373 K, employing the TG/DSC technique. Following an in situ activation at 723 K the sample was cooled to 373 K and the TG and DSC signals were stabilised before introducing 100 ml pulses of NH_3 into a N_2 stream; the injection of NH_3 continued at regular intervals until no change in sample weight was observed. The weight increase associated with the adsorption of NH_3 was used to calculate the concentration of surface acid sites while the measured enthalpy of ammonia adsorption (DSC analysis) gave a close approximation of the average strength of the accessible acid sites. Room temperature CO chemisorption was employed to characterise the supported nickel metal sites where the catalyst was cooled, following the reduction step, to 298 K in He and a fixed volume (10 μl) of CO was pulsed into the He carrier gas where the concentration of CO exiting the reactor was measured using an on-line thermal conductivity detector (TCD)

in conjunction with the JCL6000 (for Windows) data collection and manipulation package. The injection of CO was repeated until the downstream peak area was constant, indicating a surface saturation with CO. The sample was thoroughly flushed with $100 \, cm^3 \, min^{-1}$ dry He for 1 h to remove any physisorbed CO. The catalyst then underwent a temperature ramp ($25 \, K \, min^{-1}$) in $75 \, cm^3 \, min^{-1}$ dry He to 1073 K with the exiting gas stream passing through the on-line TCD, allowing a continual monitoring of the CO TPD profile. The catalyst bed temperature was independently measured and calibrated using an on-line data logging system (Pico Technology, model TC-08). Upon completion of the CO TPD sequence, a series of calibration test peaks were taken at ambient temperature to quantify the CO uptake/release; reproducibility was better than ±3%. High-resolution transmission electron microscopy (HRTEM) analysis was carried out using a Philips CM20 TEM microscope operated at an accelerating voltage of 200 kV. The specimens were prepared by ultrasonic dispersion in butan-2-ol, evaporating a drop of the resultant suspension onto a holey carbon support grid. The particle size distribution profiles presented in this study are based on a measurement of over 500 individual particles. Analysis by scanning electron microscopy (SEM) was conducted using a Hitachi S700 field emission SEM, operated at an accelerating voltage of 25 kV, where the sample was deposited on a standard aluminium SEM holder and coated with gold.

2.3. Catalytic reactor system

All catalytic reactions were carried out under atmospheric pressure, in situ immediately following the activation step, in a fixed bed reactor over the temperature range $473 \, K \leq T \leq 573 \, K$. The catalyst was supported on a glass frit and a layer of glass beads

above the catalyst bed served as a preheating zone, ensuring that the reactants reached the reaction temperature before contacting the catalyst. The reactor temperature was monitored continuously by a thermocouple inserted in a thermowell within the catalyst bed; catalyst temperature was constant to within ± 1 K. A Model 100 (kd Scientific) microprocessor controlled infusion pump was used to deliver the alcohol reactant feed via a glass/PTFE gas tight syringe and PTFE line at a fixed, calibrated, rate. The alcohol vapour was carried through the catalyst bed in a stream of dry He, the flow rate of which was monitored using a Humonics (Model 520) digital flowmeter. The catalytic measurements were made at $W/Q = 0.038\,\mathrm{g\,cm^{-3}\,h}$, where W represents the weight of anhydrous catalyst and Q is the inlet liquid volumetric feed rate; the overall gas hourly space velocity (GHSV) was varied in the range 7×10^2–$14 \times 10^3\,\mathrm{h^{-1}}$. A set of standard reaction conditions were chosen to assess the activity/selectivity of each catalyst and the reactivity of the C_6 alcohols, i.e. $T = 523$ K; $W/Q = 0.038\,\mathrm{g\,cm^{-3}\,h}$; WHSV $= 11 \times 10^3$ h. The product stream was analysed by on-line capillary chromatography using an AI Cambridge GC94 chromatograph equipped with a split/splitless injector and a flame ionisation detector, employing a DB-1 50 m $\times$ 0.20 mm i.d., 0.33 μm capillary column (J&W Scientific); data acquisition and analysis were performed using the JCL 6000 package. The gaseous stream was sampled at regular intervals by means of a heated gas-sampling valve and all interconnecting tubing was maintained at elevated temperatures to ensure that no condensation of either reactants or products occurred prior to analysis. Selectivity (S%) in terms of product x is defined as $m_x/m_{\mathrm{tot}} \times 100$, where m_x is the number of moles of x in the effluent stream and m_{tot} represents the total number of moles of product. The dehydration reaction was monitored until the zeolite displayed detrimental signs of deactivation at which point the zeolite was subjected to a reductive regeneration step. This step involved ramping the deactivated sample at 10 K min^{-1} to 723 K in a 20% v/v H$_2$/He mixture and maintaining this temperature for 16 h. The nature of any carbonaceous deposit was examined by temperature programmed oxidation (TPO). A 100 mg sample of a demineralised, deactivated catalyst was ramped (10 K min^{-1}) to 1248 K in a 5% v/v O$_2$/He mixture. The products evolved were analysed by on-line TCD and the catalyst bed temperature was

again independently monitored (Pico data logging system) and compared to that of the programmed reactor temperature; temperature deviations due to the carbon gasification reaction of up to 40 K were recorded. All the gases (He (99.99%), 20% v/v H$_2$/He (99.99%) and 5% v/v O$_2$/He (99.9%)) were supplied by BOC and were dried by passage through activated molecular sieves. Hexan-1-ol (>99%), hexan-2-ol (99%), hex-2-ene (>98%) and cyclohexanol (99%) were obtained from Aldrich Chemicals and used without any further purification. An activated carbon (Darco G-60) and a graphite sample (synthetic powder), supplied by Aldrich Chemicals were demineralised in dilute mineral acid to remove any metallic impurities before use as model carbon materials in the TPO studies.

3. Results and discussion

3.1. Characterisation of the freshly activated catalysts

The DSC profiles generated for the parent NaY, the three nickel exchanged samples and the SAC-13 composite are shown in Fig. 1; the pertinent thermogravimetric features are given in Table 2. The water content of NiNaY increased with increasing Ni loading due to the preferred Ni^{2+} octahedral co-ordination to six H$_2$O molecules in the hydrated unit cell. The elimination of water from Ni rich zeolites occurred in two distinct steps and the two peaks observed for Ni/NaY-B and Ni/NaY-C can be attributed to a loss of water from the zeolite framework (low temperature peak) and to that associated with the Ni^{2+} cations (high temperature peak). The higher temperature dehydration peak was only observed at higher Ni loadings and the peak intensity increased with increasing exchange. While an increase in Ni content was accompanied by a discernible shift in the $T_{\max}$ for the low temperature peak, all significant water loss had occurred by 523 K. A small weight loss was observed at 788 K in the case of Ni/NaY-B and Ni/NaY-C that can be attributed, based on the work of Lai and Rees [42], to a thermally induced dehydroxylation. The SAC-13 is characterised by a much lower thermal stability and, in marked contrast to the zeolitic materials, an increase in temperature 600 K was accompanied by an appre-
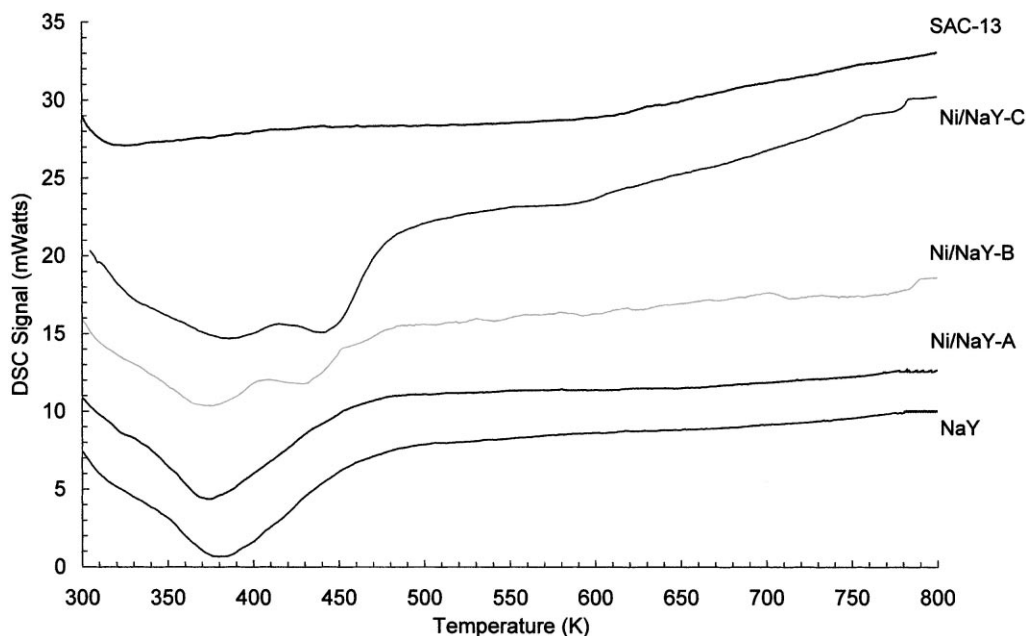
Fig. 1. The DSC profiles of the hydrated NaY, Ni/NaY and SAC-13 composite.

ciable additional weight loss due to a deformation of the supported polymer as noted by Harmer et al. [31]; the associated weight loss roughly approximates the Nafion polymeric content. In these studies, the use of SAC-13 to promote alcohol dehydration at 523 K, even for prolonged periods did not have any adverse effects on the thermal stability of the polymeric resin. Similar results were reported by Samms et al. [43] who found that sulphonic acid groups were only removed at temperatures >553 K.

The Linde Y zeolite used in this study is characterised by two independent, though interconnecting,

Table 2
Thermogravimetric analysis of the zeolite and Nafion catalyst precursors

Sample	Weight loss (%) at selected temperatures		T_{max} (K)
	523 K	873 K	
NaY	23.8	25.1	380
Ni/NaY-A	24.6	25.4	374
Ni/NaY-B	24.5	26.0	375, 440, 788
Ni/NaY-C	24.7	27.1	386, 440, 788
SAC-13	5.1	21.1	326

three dimensional networks of cavities: the accessible supercages of i.d. 1.3 nm which are linked by sharing rings of 12 tetrahedral (free diameter = 0.7–0.8 nm); the less accessible sodalite units which are linked through adjoining rings of 6 tetrahedral which form the hexagonal prisms (free diameter = 0.20–0.25 nm). The hydrogen reduction of the nickel-exchanged zeolites generates protons according to the equilibrium [39,40]

$$Ni^{2+} - Z + H_2 \rightleftharpoons Ni^0 - Z + 2H^+ - Z$$
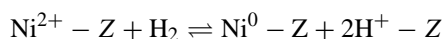
where Z represents the zeolite phase. Two surface hydroxyl groups (Brønsted acid sites) are generated for each reduced divalent Ni. The degree of Ni^{2+} reduction was determined by an iodometric titration methodology that has received a full treatment elsewhere [39] and the results are recorded in Table 3. The percentage reduction of the Ni component decreased with increasing loading, i.e. reduction was retarded with increasing proton concentration forcing the above redox equilibrium to the left. Under the stated reduction conditions, Ni^{2+} was reduced to Ni^0 and there was no evidence of a partial reduction to Ni^+ [39]. The structural hydroxyl groups generated during reduction

Table 3
Degree of Ni^{2+} reduction based on iodometric titrations and infra-red analysis and the unit cell (UC) distribution of the Brønsted acid sites that are generated in the zeolite large cages (LC) and small cages (SC)

Sample	Ni^{2+} reduction (%)			
	Iodometric titration	Infra-red analysis	LC H^+/UC	SC H^+/UC
Ni/NaY-A	83	78	7.8	<0.1
Ni/NaY-B	65	68	11.6	2.5
Ni/NaY-C	57	62	12.6	4.8

generated two infra-red bands [40]: a high frequency band vibrating in the range 3650–3630 cm^{-1} characteristic of OH groups that project into the large cavities and are readily accessible to incoming reactant molecules; a low frequency band vibrating in the range 3550–3530 cm^{-1} associated with protons located at oxygen in the hexagonal prisms that are not easily accessible. From a consideration of the data presented in Table 3, it is evident that the protons are sited predominantly in the more open supercages. At higher metal loadings the additional protons that are generated locate in less accessible sites. The Ni^{2+} reduction (%) values inferred from the IR band intensities are in good agreement with those determined by titremetric analysis (see Table 3). The acidic nature of these catalysts was also probed by monitoring the energy and weight changes associated with NH_3 chemisorption to yield an estimate of the average acid site strength and concentration [44–47]; the results are presented in Table 4. The parent NaY zeolite possesses a small number of acid sites that are weakly acidic. The exchange of 10 Na$^+$ ions per unit cell in Ni/NaY-A with 5 Ni^{2+} ions resulted in a significant increase in the

acid site concentration and a marked enhancement of acid site strength. A further increase in the level of nickel exchange resulted in a decrease in the average site strength but a corresponding increase in the acid site concentration. Indeed, the acid site concentration calculated from NH_3 uptake matches roughly the values inferred from the titremetric and spectroscopic analysis. Acid site strength in Ni exchanged Y zeolites has been shown to depend on metal loading [40,48] where the well-shielded small cage protons exhibit lower acid strengths [48]. The greater proportion of inaccessible Brønsted acidity in Ni/NaY-B and Ni/NaY-C results in lower average acid site strengths. The activated anhydrous SAC-13 composite is characterised by a lower concentration of acid sites than even the parent NaY zeolite while the acid strength is less than that associated with the Ni/NaY samples. However, in an aqueous environment the Nafion component is known to undergo swelling [4,31], enhancing acid site accessibility. The average acid strength and concentration in SAC-13 were both observed to increase when determined in an aqueous medium. This effect is of considerable significance in dehydration applications as any water generated as a by-product will interact with the Nafion leading to a swelling of the matrix and increase the number and strength of available acid sites.

Carbon monoxide chemisorption was employed as a means of characterising the supported metal sites. Under the stated treatment conditions, there is ample evidence in the literature [50] that CO adsorbs associatively on Ni, predominantly in a 1:1 stoichiometry. No CO adsorption was recorded on the activated NaY sample and uptake on Ni/NaY can be positively attributed to the presence of Ni metal. The amounts of CO adsorbed on the Ni/NaY samples are given in

Table 4
Characterisation of the acid site strength and concentration by NH_3 chemisorption (at 373 K) on the activated zeolite and SAC-13 catalysts

Sample	Average site strength (kJ mol^{-1} NH_3)	Acid site concentration (mmol g^{-1} catalyst)
NaY	14	1.0
Ni/NaY-A	117	2.1
Ni/NaY-B	99	3.7
Ni/NaY-C	76	4.5
SAC-13 (activated)	67	0.2
SAC-13[a] (activated and pre-swollen)	78	0.5

[a] Strength and acid site concentration determined in aqueous phase using a simple amine.

Table 5
Uptake of CO at 298 K and inferred nickel metal dispersion for the three activated Ni/NaY catalysts

Sample	CO adsorbed (mmol/g Ni)	Dispersion (%)
Ni/NaY-A	13.3	9
Ni/NaY-B	7.0	4
Ni/NaY-C	5.7	3

Table 5 and can be seen to decrease (per g_{Ni}) with an increase in metal loading, a feature indicative of the formation of larger metal crystallites. Indeed, the inferred degree of nickel dispersion is low and decreased at higher Ni content. Temperature programmed desorption (TPD) of CO has been used to some effect in characterising supported metal catalysts [49–53]. The desorption of CO from supported Ni has been reported to generate a small shoulder in the desorption profiles (not observed in this study) at 303 K which was ascribed to CO on the bridging sites while any higher temperature desorption peaks can be related to the removal of CO that interacts with one Ni site only [52]. The nature of the metal/support interaction(s) can significantly affect the chemisorptive properties of Ni [54] where, for instance, supporting Ni on TiO_2 has been shown to decrease the strength of CO adsorption

[55]. Hu and Ruckenstein [56] attributed CO desorption from a Ni/MgO catalyst occurring at $T < 473$ K to species that are molecularly adsorbed on smooth crystal planes while a recombination of dissociatively adsorbed C and O species on stepped Ni surfaces generated a peak at 730 K. Arena et al. [49] reported a CO desorption shoulder at 856 K and linked this to the reaction between unreduced NiO and dissociated CO. The CO TPD profiles are presented in Fig. 2 where desorption, in each case, occurred in two steps, i.e. a low (<723 K) and a high temperature (>873 K) desorption. There was no appreciable CO desorption from any of the zeolite catalysts below 573 K indicative of strongly bound CO which is diagnostic of a relatively weak Ni/zeolite interaction. As the total CO uptake on Ni/NaY-A was low the resultant desorption profile has been magnified to facilitate a direct comparison with the other profiles. At higher Ni loadings the low temperature desorption peak increased in intensity and is resolved into two components in the case of Ni/NaY-C. It is clear that a greater proportion of the CO held on Ni/NaY-A desorbed at the higher temperature suggesting a stronger interaction with CO than is apparent for Ni/NaY-B or Ni/NaY-C. It is generally agreed that the CO desorption temperature is sensitive to changes in the electronic structure of the supported
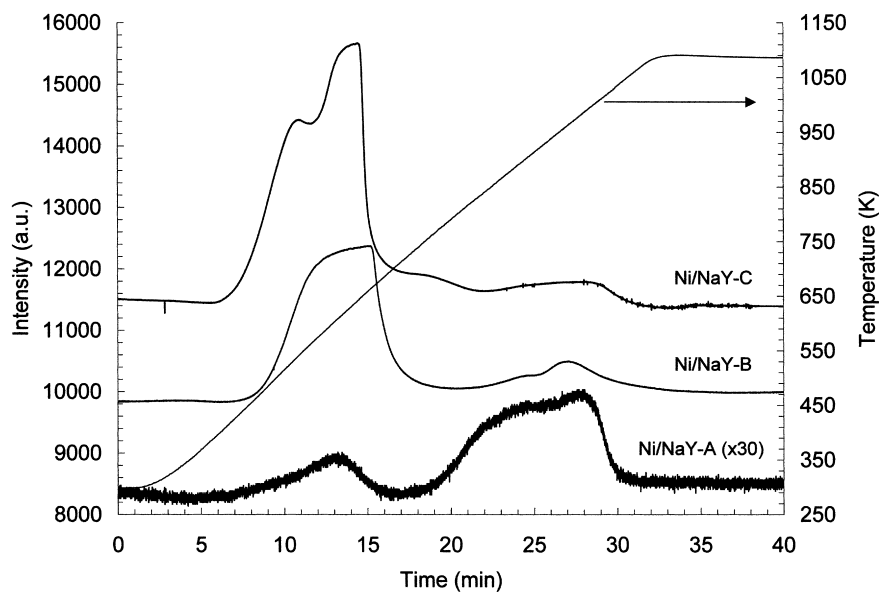

Fig. 2. The CO TPD profiles for the activated Ni/NaY catalysts.
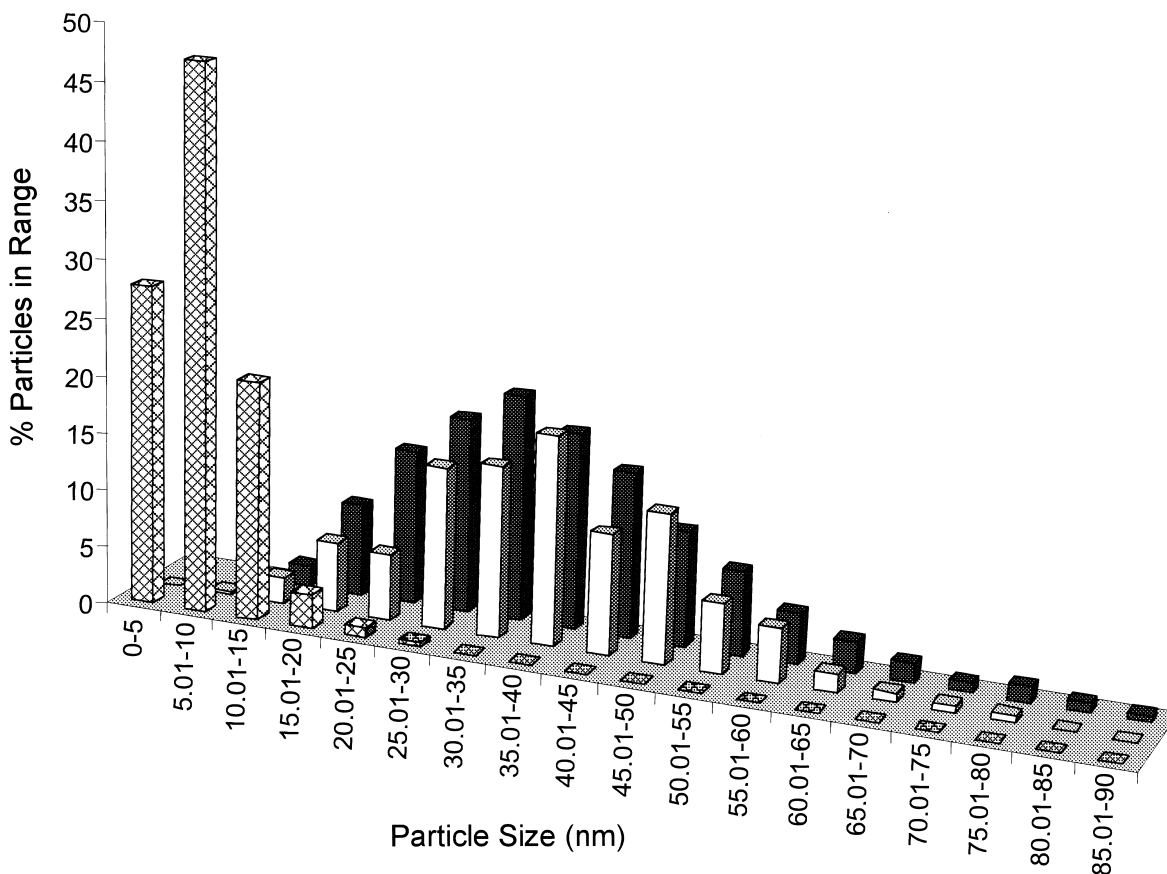
Fig. 3. Particle size distribution profiles of freshly reduced Ni/NaY-A (cross-hatched bars, $d = 8$ nm), Ni/NaY-B (open bars, $d = 37$ nm) and Ni/NaY-C (solid bars, $d = 38$ nm).

metal [50]. The greater contribution of the high temperature peak to the TPD profile for Ni/NaY-A can be attributed to an electron enrichment of the Ni particles due to the higher concentration of electron donating Na ions in the aluminosilicate framework.

The Ni particle size distribution was determined by transmission electron microscopy (TEM) and the resultant histograms are presented in Fig. 3. Each zeolite is characterised by a wide distribution of particle sizes that is more marked in the case of the two higher loaded samples. Moreover, an increase in nickel content was accompanied by an increase in the surface weighted mean particle size (*d*); the values are included in the caption to Fig. 3. The majority of the metal particles are far too large to be accommodated within the crystalline lattice and are anchored

to the external surface. On relatively thin areas of samples prepared for TEM, metal particles deposited at pore mouths and within the zeolite cage structure could be distinguished. There is, however, a smaller internal metal component that can contribute directly to the catalytic process. Typical TEM images of the freshly activated Ni/NaY-A and Ni/NaY-B are provided in Fig. 4a and b, respectively; selected area electron diffraction confirmed that the Ni particles were crystalline. The Ni crystallites are congregated along the edges of the zeolite structure and have a rounded morphology, indicative of weak metal/support interaction as inferred from the CO TPD patterns. Scanning electron microscopy analysis (SEM) highlight the pertinent topographical features of the zeolite catalysts and a representative micrograph is shown in
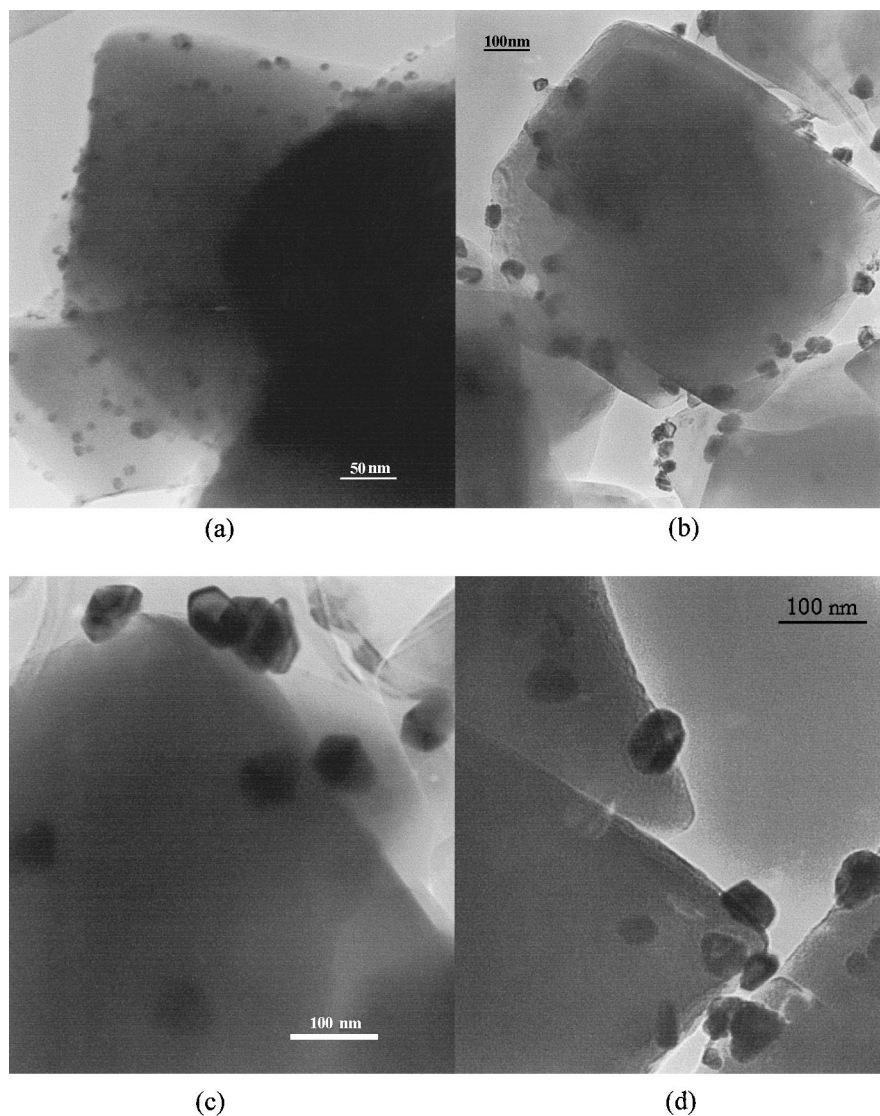
Fig. 4. (a) The TEM micrograph illustrating the morphology of the Ni crystallites on the surface of a freshly reduced Ni/NaY-A, (b) the TEM micrograph illustrating the morphology of the Ni crystallites on the surface of a freshly reduced Ni/NaY-B, (c) the TEM micrograph illustrating the morphology of the Ni crystallites on the surface of Ni/NaY-B after use in the dehydration of hexan-1-ol at 523 K; $W/Q = 0.038\,\mathrm{g\,cm^{-3}\,h}$; GHSV $= 11 \times 10^3\,\mathrm{h^{-1}}$, (d) the TEM micrograph illustrating the morphology of the Ni crystallites on the surface of Ni/NaY-B after use in the dehydration of cyclohexanol at 523 K; $W/Q = 0.038\,\mathrm{g\,cm^{-3}\,h}$; GHSV $= 11 \times 10^3\,\mathrm{h^{-1}}$.

Fig. 5a. The geometric structural features associated with zeolite Y are readily apparent while the nature of nickel metal dispersion on the surface is also evident. The particle size distributions derived from SEM images were consistently higher than those generated from the TEM treatment, e.g. $d = 52\,\mathrm{nm}$ as opposed to 37 nm in the case of Ni/NaY-B. This deviation in size can be attributed, in part, to the method of sample preparation where a coating of the specimen with a thin layer of gold to avoid sample charging may serve to partially obscure some of the surface metal.
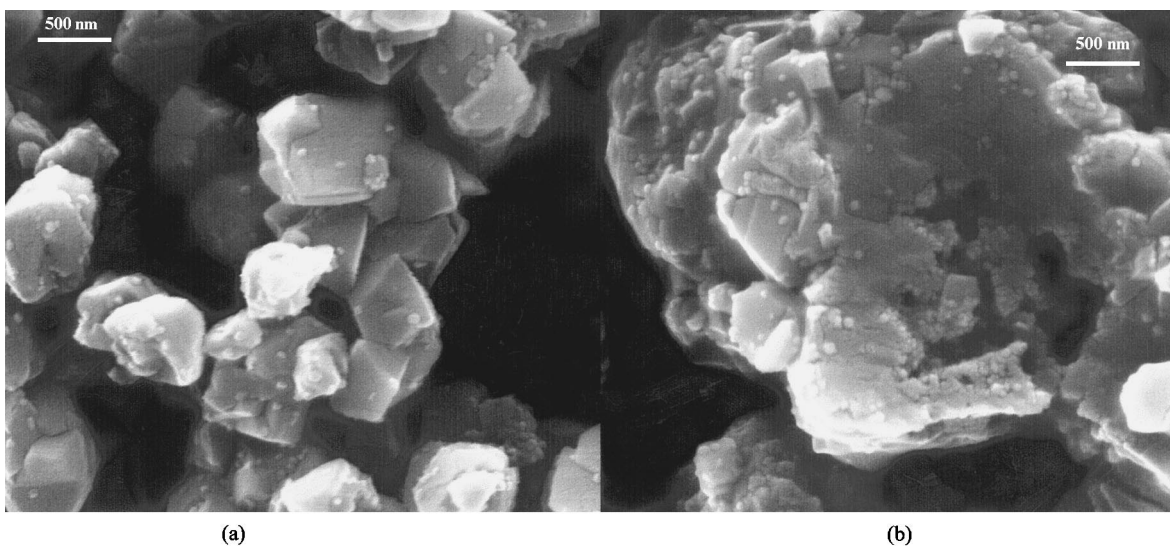
Fig. 5. (a) The SEM micrograph depicting the topographical features of freshly activated Ni/NaY-B, (b) the SEM micrograph depicting the topographical features of Ni/NaY-B after use in the dehydration of hexan-1-ol at 523 K.

3.2. Catalytic dehydration

The conversion of hexan-1-ol over all the activated catalysts generated hex-1-ene, hex-2-ene, hex-3-ene, 1,1-dihexyl ether, hexanal and hexane as products. The formation of alkenes involves a protonation of the alcohol by the surface Brønsted acid sites, a slow dissociation into a carbonium ion and a fast expulsion of the hydronium ion to form the alkene. It is typical in dehydration reactions for one isomeric form of the alkene to predominate and, from a consideration of reaction equilibrium constants [57], hex-2-ene is the thermochemically preferred isomer. The generation of hexyl ether is the result of a condensation reaction involving, from the standpoint of conventional organic chemistry [58], nucleophilic substitution with the protonated alcohol as substrate and the second hexan-1-ol molecule as the nucleophile. The catalysts used in this study generated the symmetrical 1,1-dihexyl ether as, by far, the major ether product but trace amounts ($S <$ 0.1%) of the unsymmetrical 1,2-ether were also detected. The conversion of hexan-1-ol over the parent NaY resulted in a low fractional conversion (x) primarily to hexanal but 1,1-dihexyl ether ($S < 15\%$) was also detected in the product stream where $t <$ 1 h. Jacobs et al. [21,59] similarly noted a dehydro-

genation of isopropanol over alkali metal exchanged X and Y zeolites. The degree of conversion was observed to decline with time-on-stream as shown in Fig. 6; hexan-1-ol conversions, at two selected times (0.5 and 4 h), over freshly activated and regenerated samples are listed in Table 6 for comparative purposes. Del Castillo and Grange [60] observed a decline in butan-1-ol conversion over a Ti montmorillonite clay due to coking. Deactivation of zeolites is typically due [61,62] to the retention of products from side reactions in the narrow internal pore structure, which occlude the active sites from the incoming reactant. In the case of acid catalysis, the rapid accumulation of coke has been associated with unsaturated hydrocarbons that readily undergo bimolecular reactions to generate detrimental carbonaceous residues [62]. As alkenes represent primary products in this particular system the formation of carbonaceous deposits on the zeolite and the subsequent deactivation is not surprising. Deactivation or inhibition of dehydration reactions has also been attributed by Thornton and Gates [24] and Ballantine et al. [25], to a hydration of the surface Brønsted acidity by the water that is produced. The HY sample, in comparison with the parent NaY, realised a considerably higher fractional conversion but underwent appreciable deactivation over the first
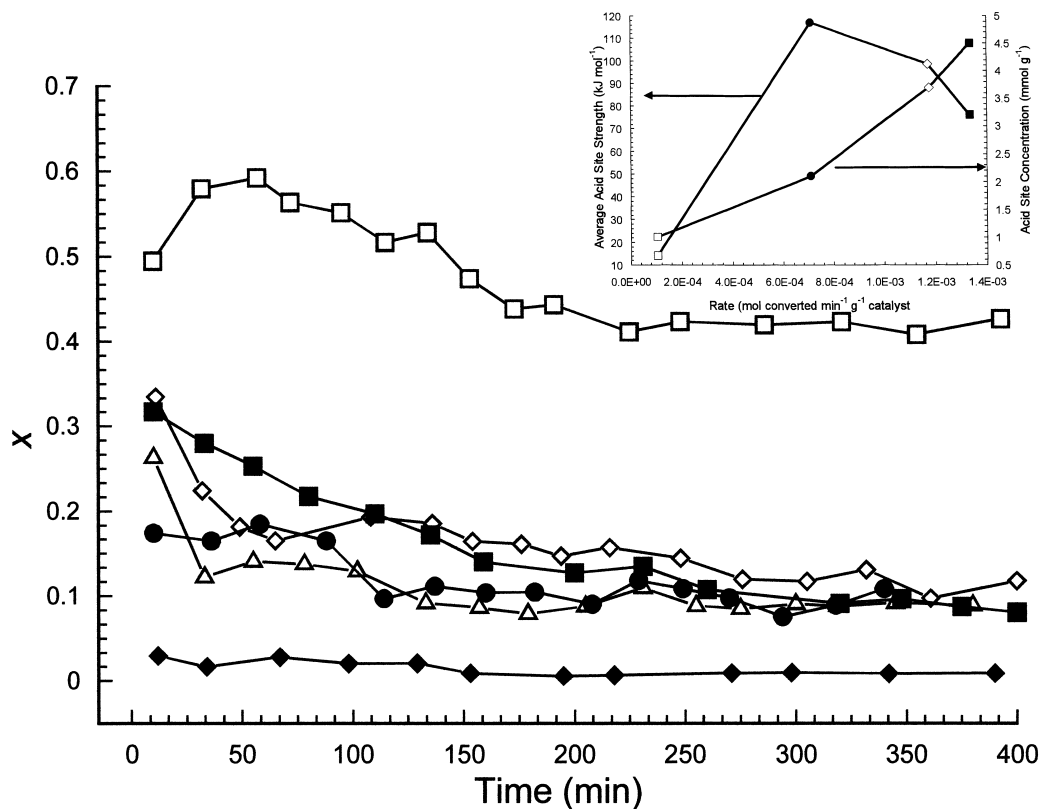
Fig. 6. Fractional conversion (x) of hexan-1-ol with time on stream over HY ($\diamond$), NaY ($\blacklozenge$), Ni/NaY-A ($\bullet$), Ni/NaY-B ($\blacksquare$), Ni/NaY-C ($\triangle$) and SAC-13 ($\square$): $T = 523$ K; $W/Q = 0.038$ g cm^{-3} h; GHSV $= 11 \times 10^3$ h^{-1}. Inset: relationship between dehydration rate and acid site strength and concentration, symbols as above.

80 min on-stream; dehydration was primarily to hexenes with a low selectivity ($<5\%$) in terms of ether formation.

The Ni/NaY samples all exhibited appreciably higher activities than the parent NaY and again a marked decline in conversion with time-on-stream was observed (see Fig. 6). The preferred product over Ni/NaY-A was hex-2-ene with a selectivity (ca. 40%) that was largely time invariant, as illustrated in Fig. 7a. Initially, the formation of 1,1-dihexyl ether was equivalent to both hex-1-ene and hex-3-ene but ether production dropped with time-on-stream to such an extent that only trace quantities were isolated in the product after 5 h. This decline in ether formation coincides with the overall loss of activity (see Fig. 6 and Table 6), diagnostic of a selective deactivation of the

sites involved in promoting the alcohol condensation step. The predominant product over Ni/NaY-B was again the thermodynamically favoured hex-2-ene with an initial selectivity in excess of 50% that fell slightly with time as the formation of the ether increased (see Fig. 7b). In contrast to Ni/NaY-A, the formation of hex-3-ene was preferred over hex-1-ene while the production of 1,1-dihexyl ether was not initially favoured. Under the same reaction conditions, hex-2-ene, when used as the feedstock, underwent isomerisation primarily ($S > 69\%$) to hex-3-ene with hex-1-ene as a secondary product. Given the mismatch of product selectivities from the hexan-1-ol feed where hex-2-ene was a major product, it is unlikely that the ultimate alkene product selectivity arose from a subsequent isomerisation but rather as a direct product of alcohol

Table 6
Fractional conversion (x) of hexan-1-ol over the freshly activated and regenerated zeolite and Nafion catalysts at (i) 0.5 h and (ii) 4 h: $T = 523\,K$; $W/Q = 0.038\,g\,cm^{-3}\,h^{-1}$; GHSV = $11 \times 10^3\,h^{-1}$

| | x | | | | | | | | | | | |
| | HY | | NaY | | Ni/NaY-A | | Ni/NaY-B | | Ni/NaY-C | | SAC-13 | |
	(i)	(ii)	(i)	(ii)	(i)	(ii)	(i)	(ii)	(i)	(ii)	(i)	(ii)
Reaction 1	0.22	0.14	0.03	0.01	0.17	0.11	0.28	0.14	0.26	0.09	0.58	0.42
Regeneration 1	0.20	0.08	0.01	0.01	0.12	0.09	0.17	0.09	0.15	0.04		
Regeneration 2							0.13	0.03	0.13	0.03		
Regeneration 3							0.11	0.03				

dehydration. This result is in keeping with the work of Lombardo et al. [63] who concluded that dehydration was promoted to a far greater degree over zeolites than isomerisation. Dehydration over Ni/NaY-C was
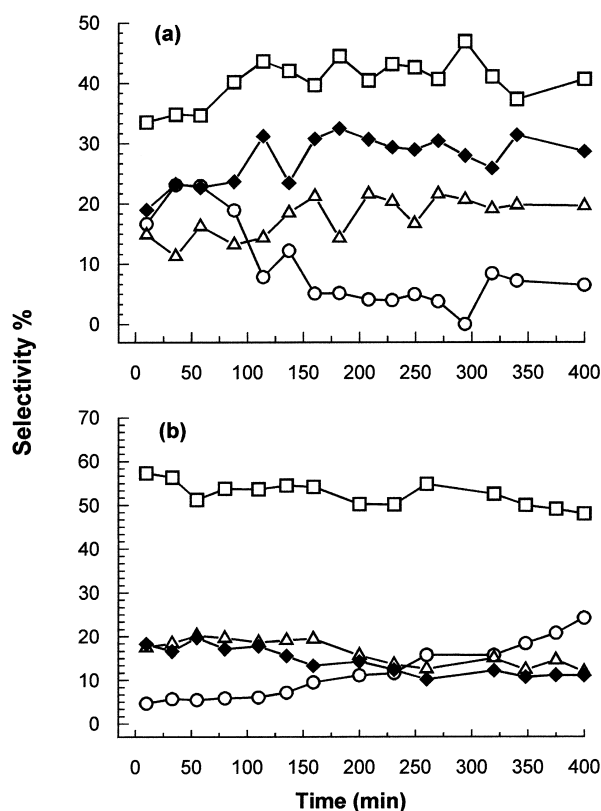

Fig. 7. Product selectivity as a function of time for the conversion of hexan-1-ol over (a) Ni/NaY-A and (b) Ni/NaY-B: hex-1-ene (◆), hex-2-ene (□), hex-3-ene (△) and 1,1-dihexyl ether (○): $W/Q = 0.038\,g\,cm^{-3}\,h$; $T = 523\,K$; GHSV = $11 \times 10^3\,h^{-1}$.

again characterised by a loss of activity (Fig. 6) and the product distribution was very similar to that delivered by Ni/NaY-B. The drop in activity as a function of time-on-stream can be quantified by extrapolation to the initial value using the empirical relationship

$$x = x_{initial} \exp(-\alpha t)$$

where the coefficient α is a measure of the degree of catalyst deactivation. The order of decreasing initial fractional conversion ($x_{initial}$), under the stated standard process conditions, follows the sequence: HY (0.42) > Ni/NaY-C (0.37) > Ni/NaY-B (0.33) > Ni/NaY-A (0.20) > NaY (0.03). The zeolite (Ni/NaY-A) that possessed the strongest acid sites, albeit fewer in number, realised a lower activity than the catalyst (Ni/NaY-C) possessing the lowest acid strength but highest concentration of sites (see Table 4). Indeed, there is a direct relationship between dehydration rate and acid site concentration as revealed in the inset to Fig. 6 while an increase in acid strength was not necessarily accompanied by a higher rate. This suggests that strong acid sites are not a prerequisite to catalyse this reaction, an assertion that finds support in the work of Jacobs [12]. Stronger acid sites may in fact be detrimental in that catalyst deactivation is typically more extreme over highly acidic samples [62]. This is also the case in this study where the deactivation coefficient, α, increased in the order: NaY ($9 \times 10^{-4}\,min^{-1}$) < Ni/NaY-A ($33 \times 10^{-4}\,min^{-1}$) < Ni/NaY-B ($50 \times 10^{-4}\,min^{-1}$) < Ni/NaY-C ($58 \times 10^{-4}\,min^{-1}$). The conversion of hexan-1-ol over Nafion was characterised by an initial induction period wherein activity increased, followed by a gradual decline in conversion (see Fig. 6); the Nafion/SiO$_2$ composite delivered significantly higher

Table 7
Product selectivity in terms of hexene(s) (S_{hexene}) formation over the freshly activated and regenerated zeolite and freshly activated Nafion catalysts at (i) 0.5 h and (ii) 4 h: $T = 523$ K; $W/Q = 0.038$ g cm^{-3} h; GHSV $= 11 \times 10^3$ h^{-1}

| | $S_{hexene(s)}$ [a] | | | | | | | | | | | |
| | HY | | NaY [b] | | Ni/NaY-A | | Ni/NaY-B | | Ni/NaY-C | | SAC-13 | |
	(i)	(ii)	(i)	(ii)	(i)	(ii)	(i)	(ii)	(i)	(ii)	(i)	(ii)
Reaction 1	91	>99	0	0	65	90	86	82	82	80	91	95
Regeneration 1	90	>99	0	0	56	88	83	80	90	92		
Regeneration 2							76	78	85	94		
Regeneration 3							72	76				

[a] Hex-1-ene + hex-2-ene + hex-3-ene.
[b] Hexanal and 1,1-dihexyl ether are the only products.

fractional conversions (see also Table 6). The presence of water vapour as a product can serve to solvate the polymeric Nafion particles that then swell making previously inaccessible sites available to the alcohol reactant. As this swelling effect is time dependent, this may explain why the SAC-13 sample does not exhibit the dramatic loss of activity associated with the zeolites in that the detrimental effect of any coke deposition is counterbalanced to some degree by a freeing of active sites through swelling. The Nafion resin has been observed to be an inefficient catalyst for reactions where the conditions do not favour a swelling of the polymeric framework [34,64]. This phenomenon is highlighted in Table 4 where the acid site concentration in the activated and preswollen SAC-13 composite was more than double that of the activated but dehydrated sample.

The reductive regeneration employed in this study was only effective in partially restoring activity (see Table 6). With each successive regeneration/reaction cycle, the overall conversion was observed to decline albeit to a noticeably lesser degree after the first cycle of regeneration/reuse. Catalyst regeneration studies were limited to the zeolitic materials due the thermal instability of the Nafion composite at elevated temperatures. A progressive catalyst deactivation was typically accompanied by an increase in hexene(s) selectivity (see Table 7), i.e. as a general observation the sites responsible for alcohol condensation were more prone to deactivation. It is generally agreed [21,65,66] that dehydration selectivity is dependent on the nature of the surface acidity. Kooli and Jones [65] and Del Castillo and Grange [60] correlated primary alcohol

dehydration activity over activated clays with surface Brønsted acidity where the clays with the highest level of acidity realised the lowest selectivity in terms of alkene formation. In this study, each Ni/NaY, the fully protonated HY and SAC-13 catalyst all preferentially promoted the formation of alkenes and this selectivity was maintained after the reductive regeneration.

The dehydration of cyclohexanol over NiNaY-B under the same standard conditions yielded cyclohexene as the predominant product ($S > 90\%$) with cyclohexane only detected over the first 1.5 h on-stream. Catalysis over the zeolite samples was again characterised by a time dependent deactivation; the α value (see Table 8) for Ni/NaY-B was more 10 times greater than that recorded for the dehydration of hexan-1-ol. The regenerated catalyst again delivered a lower initial activity than that recorded for the fresh sample. Cruz Costa et al. [30] also reported that, at similar reaction temperatures, cyclohexene was the dominant product over a zirconium phosphate catalyst. Since cyclohexanol possesses an equatorial C–OH bond, a perpendicular approach to the catalyst surface is favoured over a flat orientation as the less sterically hindered route to the Brønsted acid sites. Cleavage of the C–O bond yields a carbocation intermediate that undergoes further rearrangement yielding cyclohexene. Dicyclohexyl ether formation has been reported by Chatterjee et al. [67] (bentonite clay) and Olah et al. [5] (Nafion); at no time was any ether product isolated in the exit stream from the zeolite and SAC-13 catalysts. The conversion of the secondary C$_6$ alcohol, hexan-2-ol, yielded an initial dehydration rate that was significantly higher than that recorded for hexan-1-ol (see

Table 8
Initial fractional conversion ($x_{initial}$) of three C_6 alcohols over freshly activated and regenerated Ni/NaY-B; $T = 523$ K; $W/Q = 0.038$ g cm^{-3} h; GHSV $= 11 \times 10^3$ h^{-1}

	Hexan-1-ol		Hexan-2-ol		Cyclohexanol	
	$x_{initial}$	$10^3 \, \alpha$ (min^{-1})	$x_{initial}$	$10^3 \, \alpha$ (min^{-1})	$x_{initial}$	$10^3 \, \alpha$ (min^{-1})
Freshly activated	0.33	5	0.46	16	0.71	53
Regenerated	0.19	11	0.28	10	0.34	13

Table 8). In synthetic organic chemistry, it is well established [58] that alcohol dehydration follows a reactivity sequence, tertiary > secondary > primary, that represents the decreasing rate of carbonium ion formation. The symmetrical 2,2-dihexyl ether was the only appreciable ether product and hex-2-ene was again the favoured alkene isomer. The dehydration of the secondary alcohol was characterised by a greater degree of deactivation and a higher alkene/ether ratio than that recorded for hexan-1-ol. The alcohol to ether route is known [25,68] to be effective only with primary alcohols and elimination to form alkenes is the principal reaction that occurs with secondary and tertiary alcohols.

The effect of varying reaction temperature on the time dependent hexan-1-ol conversion is shown in Fig. 8. The extracted initial dehydration rate increased with increasing temperature from 9.2×10^{-4} mol min^{-1} g^{-1} (473 K) to 1.8×10^{-3} mol min^{-1} g^{-1} (573 K). This increase in activity was also accompanied by a greater degree of deactivation as the value of α was raised from 473 K (3×10^{-4} min^{-1}) to 573 K (11×10^{-3} min^{-1}), i.e. concomitant with the increase in initial dehydration rate at elevated temperatures was the increase in coke deposition leading to deactivation. The effect of temperature on the initial alkene/ether product ratio is illustrated in the inset to Fig. 8 where the progressive shift to selective alkene
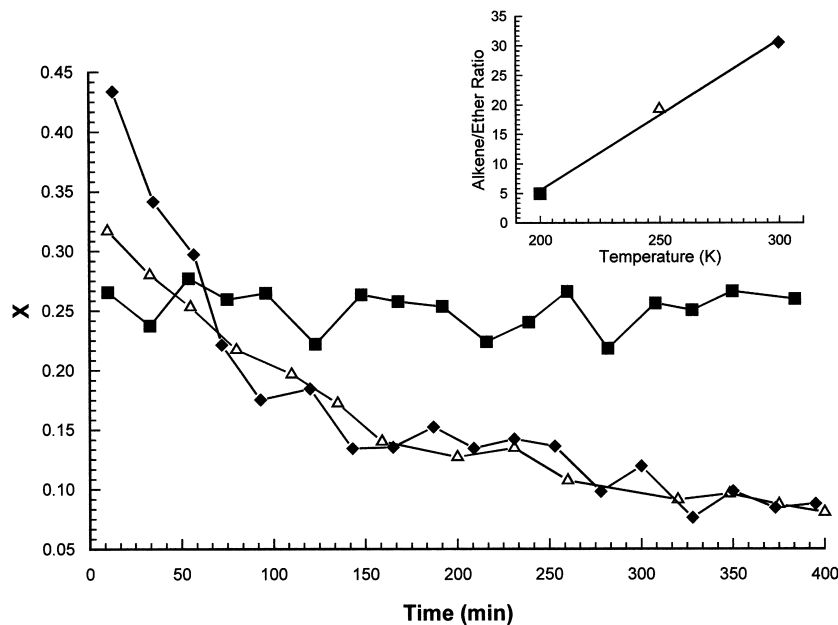

Fig. 8. Time dependant fractional conversion (x) of hexan-1-ol over Ni/NaY-B at 473 K (■), 523 K (△) and 573 K (◆): $W/Q = 0.038$ g cm^{-3} h; GHSV $= 11 \times 10^3$ h^{-1}. Inset: effect of temperature on the initial alkene/ether product ratio, symbols as above.

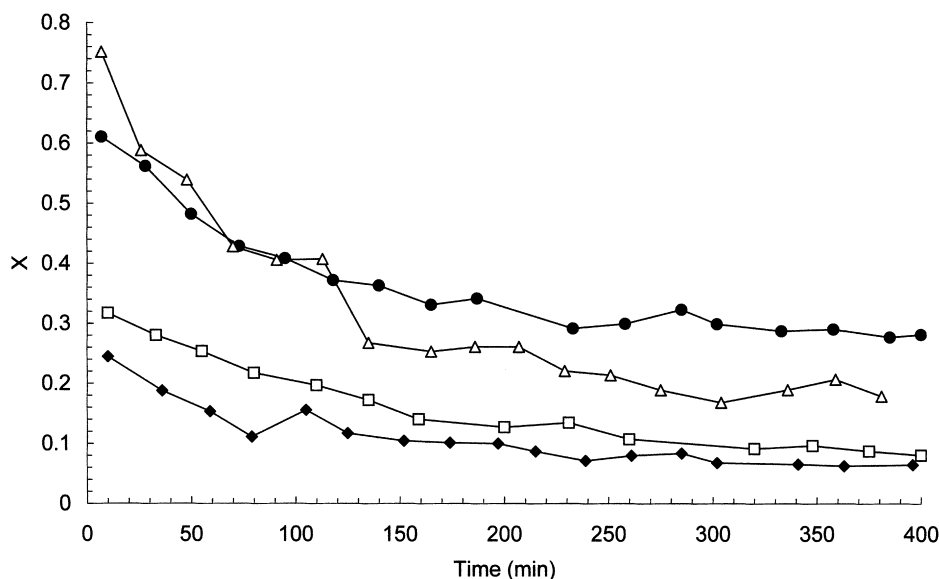Fig. 9. Time dependant fractional conversion (x) of hexan-1-ol over Ni/NaY-B at GHSV $= 56 \times 10^2\,h^{-1}$ ($\bullet$), $83 \times 10^2\,h^{-1}$ ($\triangle$), $14 \times 10^3\,h^{-1}$ ($\square$) and $11 \times 10^3\,h^{-1}$ ($\blacklozenge$): $T = 523\,K$; $W/Q = 0.038\,g\,cm^{-3}\,h$.

formation with increasing reaction temperature is clearly evident. This phenomenon finds support in earlier studies using liquid [68] and solid [5,22] inorganic acids where elimination to yield the alkene was observed to predominate at high temperatures. Altering the GHSV and, consequently, the contact time also had an impact on activity where an increase in GHSV was accompanied by a drop in conversion as shown in Fig. 9; the associated $x_{initial}$ values fell from 0.63 to 0.26. The drop in initial activity was more pronounced at GHSV $> 11 \times 10^3\,h^{-1}$ and at lower velocities dehydration activity was essentially constant. Such an increase in conversion at greater contact times in the case of a microporous catalyst can be attributed, at least in part, to pore diffusional constraints. Alterations to the GHSV did not result in any appreciable change to the selectivity patterns and alkene formation was consistently dominant.

3.3. Characterisation of the used catalysts

The nature of carbon deposition in the deactivated zeolites was probed by means of temperature programmed oxidation (TPO) where the original Ni metal content was removed by a demineralisation

treatment to ensure that gasification of carbon was not catalysed by any residual Ni. Under identical reaction conditions the carbon content of NiNaY decreased in the order: Ni/NaY-C (40% w/w) > Ni/NaY-B (28% w/w) > NiNaY-A (12% w/w) > NaY (3% w/w). This sequence follows that of decreasing acid site concentration (see Tables 3 and 4), indicating that coke formation, in common with dehydration activity is dependent on the number rather than strength of available acid sites. There is a direct link between carbon content in the used zeolites and the magnitude of the deactivation coefficients quoted above which supports the contention that deactivation is the result of a carbonaceous lay down that occludes the active sites. The main dehydration reaction and coke formation can be viewed as parallel processes. The degree of coke deposition was dependent on the reactant/reaction conditions and carbon contents of up to 50% w/w were recorded for the deactivated zeolites. Selected TPO profiles are provided in Fig. 10, taking Ni/NaY-B as a representative catalyst. The TPO profiles of amorphous and graphitic carbon were also generated as benchmarks against which the catalytically generated carbon can be compared; the characteristic T_{max} values are included in Table 9. It is well
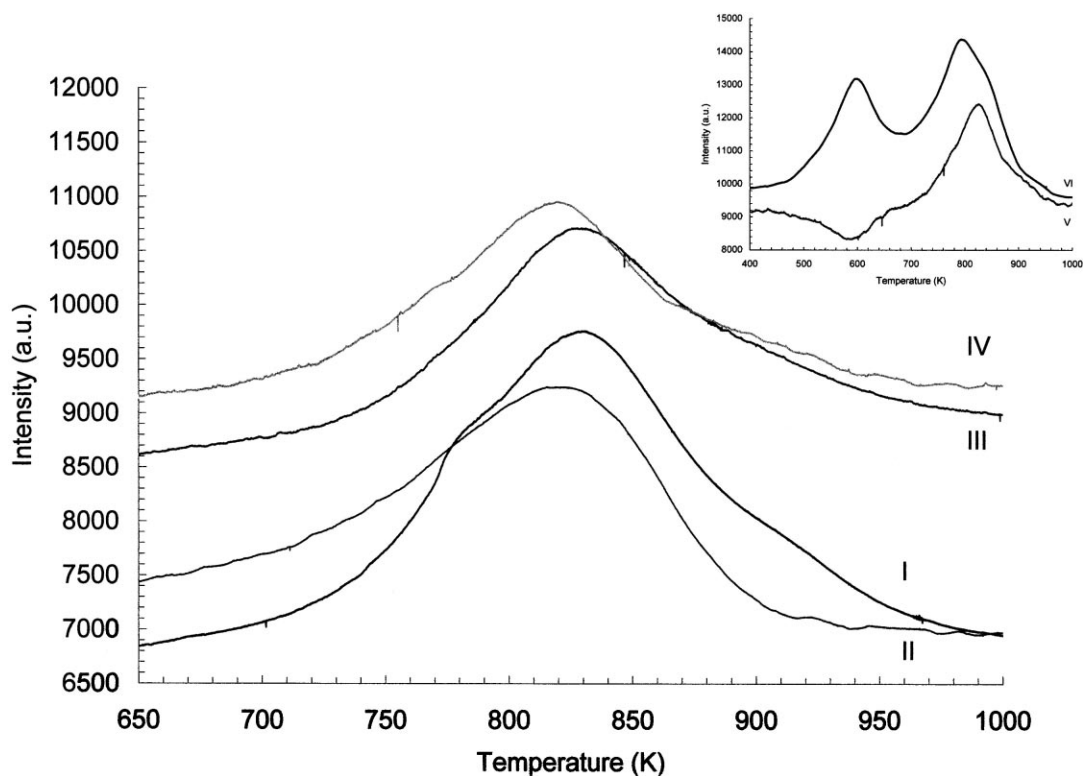
Fig. 10. The TPO profiles generated from a sample of Ni/NaY-B after 8 h on stream (I), following regeneration (II), one cycle of regeneration and reuse (III) and three cycles of regeneration/reuse (IV): hexan-1-ol feedstock; $T = 523$ K; $W/Q = 0.038$ g cm^{-3} h; GHSV $= 11 \times 10^3$ h^{-1}. Inset: the TPO profiles generated from deactivated Ni/NaY-C (V) and HY (VI).

Table 9
Summary of the TPO data generated from deactivated/regenerated Ni/NaY and model carbon materials

Catalyst/reactant		T_{max} (K)	Carbon content (%)
Ni/NaY-B/hexan-1-ol	Deactivated no regeneration	831	37
	Regenerated	822	12
	1 Regeneration/reuse	827	28
	3 Regenerations/reuses	821	25
	GHSV $= 56 \times 10^2$ h^{-1}	884	30
	GHSV $= 11 \times 10^3$ h^{-1}	831	37
	GHSV $= 14 \times 10^3$ h^{-1}	882	48
Ni/NaY-B/cyclohexanol	Regenerated	823	19
Ni/NaY-C/hexan-1-ol	Regenerated	830	40
HY/hexan-1-ol	Deactivated	596, 795	15
Amorphous carbon		821	
Graphite		1141	

established that an increasing order in carbon structure, i.e. a move from an amorphous to a graphitic nature is accompanied by an increase in the temperature at which gasification is initiated [69]. The TPO profile (I) generated from Ni/NaY-B that had been on stream for 8 h (at which point dehydration activity had dropped by a factor of 4) is characterised by a broad peak that bears two shoulders. The lower temperature shoulder (ca. 773 K) is indicative of a highly amorphous structure while the higher temperature shoulder (ca. 908 K) suggests the presence of a more ordered carbon. A regeneration of Ni/NaY-B yielded a profile (II) where the oxidation maximum was shifted to a lower temperature and the shoulders observed prior to regeneration are no longer present. Regeneration served to remove deleterious coke deposits, particularly the "more ordered" form(s). Upon reuse of this regenerated catalyst the resultant TPO profile (III) was dominated by a broad peak with no distinguishable shoulders. The TPO profile (IV) associated with a Ni/NaY-B sample that had been through three cycles of regeneration/reuse is likewise extremely broad with no secondary peak(s) or shoulder(s). The residual carbon that remained after the regeneration did block active sites available on the freshly activated sample with a resultant decrease in both dehydration activity and the formation of a more ordered carbon deposit. In keeping with the results presented, here, Larsen et al. [70], when studying the dehydration of low-molecular weight alcohols, observed that Y zeolites were more likely to form greater amounts of "harder" coke than was the case with tungstated zirconia. The coke deposited on HY gave a TPO profile dominated by two distinct T_{max} values (see Table 9) that were both lower than the values generated for deactivated Ni/NaY. Indeed, a direct comparison of the TPO profiles for HY and Ni/NaY-C in the inset to Fig. 10 clearly shows that the presence of Ni limits the lay down of highly amorphous carbon. It has been shown elsewhere [71] that the presence of Ni metal can prolong zeolite lifetime by hydrogenating/dehydrogenating coke precursors and so inhibit carbon deposition.

The average Ni particle size increased in every instance after the dehydration reaction: the observed change in particle size is recorded in Table 10. The progressive shift in size distribution to larger values with extended catalyst use is well illustrated by the histograms in Fig. 11; the mean Ni diameter is

Table 10

Surface weighted mean nickel particle sizes (*d*) of freshly activated and used Ni/NaY samples: feedstock = hexan-1-ol; $T = 523$ K; $W/Q = 0.038$ g cm^{-3} h; GHSV = 11×10^3 h^{-1}

Sample	*d* (nm)	
	Freshly reduced	Used
Ni/NaY-A	8	12
Ni/NaY-B	37	46
Ni/NaY-C	38	49

identified in the Fig. caption. Zeolite supported Ni is known to be highly mobile and can readily sinter to form larger metal particles on the external surface [72,73]. Moreover, an increase in reaction temperature also served to increase further the average particle size (see Table 11). As the Ni crystallites in the freshly activated samples do not display any of the classical signs of strong metal/support interaction, an increase in reaction temperature must raise the mobility of these crystallites leading to the observed particle growth. Representative TEM images of Ni/NaY-B after use in the dehydration of hexan-1-ol and cyclohexanol are shown in Fig. 4c and d, respectively. In addition to the increase in the Ni particle size, the crystallite morphology was also subject to change in that the particles adopted a more defined geometrical shape. This reconstruction was observed for all reactions involving both primary and secondary C_6 alcohol reactants regardless of the process conditions. A representative SEM of a used zeolite catalyst is shown in Fig. 5b wherein the growth of Ni crystallites during catalysis is again in evidence. The clustering of Ni particles around the pore mouth openings suggests a migration of Ni from intracrystalline locations. A restructuring of Ni surfaces during chemisoption of organic molecules is well documented [74,75]. The migration of Ni particles on a zeolite substrate was observed by Gallezot et al. [76] to be dependent on the nature of the adsorbed molecules and on the degree of hydration of the zeolite framework. It is possible that the water generated in this reaction resulted in a rehydration of the zeolite lattice, which induced a degree of mobility of the metal crystallites.
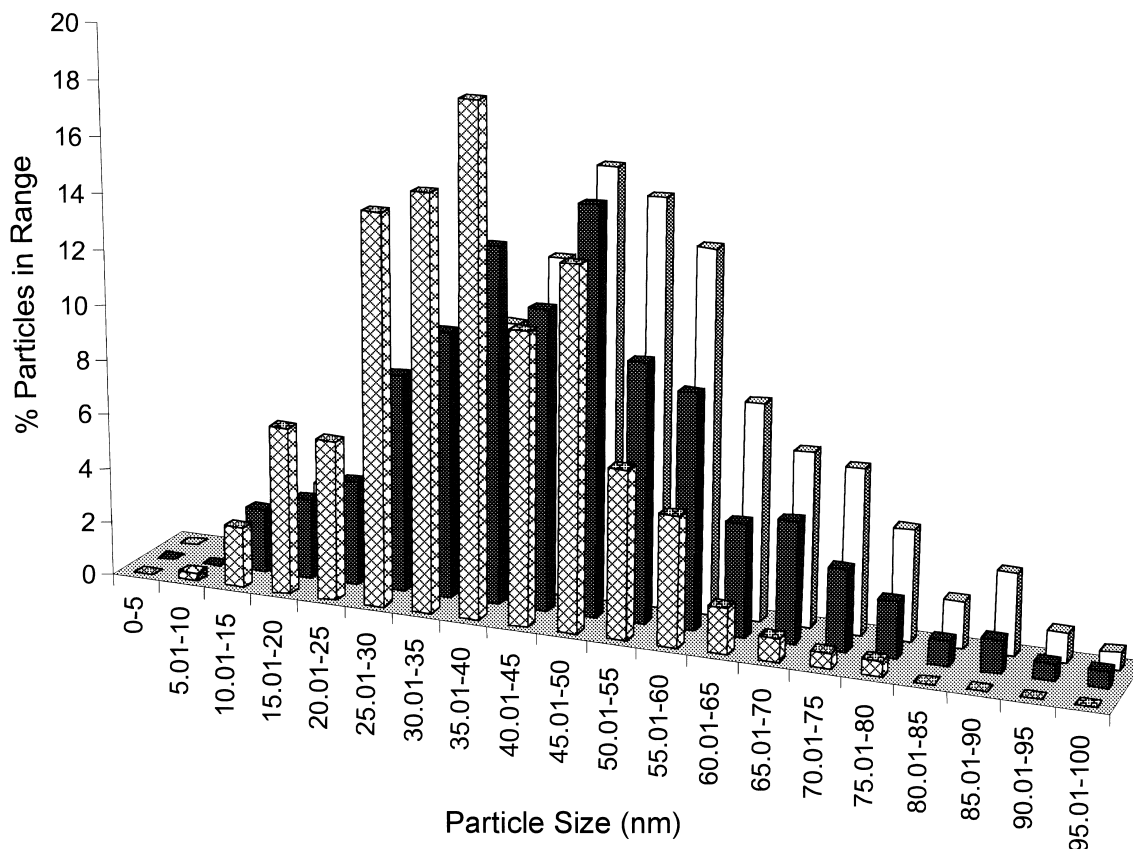
Fig. 11. Particle size distribution profiles of freshly reduced Ni/NaY-B (cross hatched bars, $d = 37$ nm), Ni/NaY-B after 8 h on stream (solid bars, $d = 46$ nm) and NiNaY-B after three cycles of regeneration/reuse (open bars, $d = 51$ nm); feedstock = hexan-1-ol; $T = 523$ K; $W/Q = 0.038$ g cm^{-3} h; GHSV = 11×10^3 h^{-1}.

Table 11
Variation in the surface weighted mean nickel particle size (d) of Ni/NaY-B with increasing reaction temperature in the dehydration of hexan-1-ol; $W/Q = 0.038$ g cm^{-3} h; GHSV = 11×10^3 h^{-1}

Reaction temperature (K)	d (nm)
Freshly reduced	37
473	40
523	46
573	49

4. Conclusions

Reduction of Ni^{2+} cations supported on NaY generates surface Brønsted acidity that serves to promote the dehydration of hexan-1-ol principally to hexene(s) (with hex-2-ene as the predominant isomer); condenstion to form 1,1-dihexyl ether is a secondary reaction. Dehydration activity is a function of the number of available surface Brønsted acid sites rather than acid strength. An increase in the Ni content raised the fractional conversion due to the accompanying increase in acid site concentration and the highest loaded Ni/NaY delivered comparable conversions to a fully protonated HY. The Ni/NaY and Nafion based catalysts all promoted the preferential production of hexenes from hexan-1-ol and the alkene/ether ratio in the product stream was raised at elevated temperatures. The dehydration of hexan-2-ol yielded 2,2-dihexyl ether and hex-2-ene as the predominant products while cyclohexanol was converted largely to cyclohexene with trace amounts of cyclohexane: reactivity

increased in the sequence hexan-1-ol < hexan-2-ol < cyclohexanol. Deactivation by coke deposition was common to all the zeolite catalysts where deactivation is a function of acid site concentration and the presence of Ni limits the deposition of highly amorphous carbon. In contrast to the zeolites, the Nafion sample exhibited an initial increase in conversion with time that is attributed to a solvation of the polymeric matrix by the water vapour product which served to swell the resin rendering previously inaccessible sites available to the alcohol reactant. Regeneration of the spent zeolite in a reductive environment was found to partially restore catalytic activity by removing an appreciable component of the entrapped amorphous coke. The Ni particle size distribution for each zeolite was shifted to higher values after catalysis. The Ni/NaY samples are characterised by relatively weak metal/support interaction(s) and Ni crystallites mobility can be induced by a direct interaction with the alcohol reactant or a framework rehydration during catalysis.

References

[1] A. Chénedé, N. Abd. Rahman, I. Fleming, Tetrahedron Lett. 38 (1997) 2381.
[2] V.J. Frilette, E.B. Mower, M.K. Rubin, J. Catal. 3 (1964) 25.
[3] B.C. Gates, J.S. Wisnouskas, H.W. Heath, J. Catal. 24 (1972) 320.
[4] G.A. Olah, P.S. Iyer, G.K.S. Prakash, Synthesis (1986) 514.
[5] G.A. Olah, T. Shamma, G.K.S. Prakash, Catal. Lett. 46 (1997) 1.
[6] F.P. Heese, M.E. Dry, K.P. Möller, Catal. Today 49 (1999) 327.
[7] F. Ancilotti, M. Massi Massuri, E. Pescarollo, J. Catal. 46 (1977) 49.
[8] F. Ancilotti, M. Massi Massuri, E. Pescarollo, J. Mol. Catal. 4 (1978) 37.
[9] D. Kalló, R.M. Mihályi, Appl. Catal. A 121 (1995) 45.
[10] H. Pines, J. Manassen, Adv. Catal. 16 (1966) 49.
[11] P.A. Venuto, P.S. Landis, Adv. Catal. 18 (1968) 259.
[12] P.A. Jacobs, Carboniogenic Activity of Zeolites, Elsevier, Amsterdam, 1977, p. 99.
[13] R. Rudham, A. Stockwell, Catalysis, Vol. 1, Specialist Periodical Reports, The Chemical Society, London, 1977, p. 87.
[14] R. Rudham, A. Stockwell, in: B. Imelik (Ed.), Catalysis by Zeolites, Elsevier, Amsterdam, 1980, p. 113.
[15] R.A. Schoonheydt, L.J. Vandamme, P.A. Jacobs, J.B. Uytterhoeven, J. Catal. 43 (1976) 292.
[16] B. Shi, H.A. Dabbagh, B.H. Davis, J. Mol. Catal. A: Chem. 141 (1999) 257.
[17] M.T. Aronson, R.J. Gorte, W.E. Farneth, J. Catal. 98 (1986) 434.
[18] F.S. Stone, A.L. Agudo, Z. Phys. Chem. 64 (1969) 161.
[19] K.V. Topchieva, H.C. Tuang, Kinet. Katal. 14 (1973) 398.
[20] S.J. Gentry, R. Rudham, J. Chem. Soc., Faraday Trans. I 70 (1974) 1685.
[21] P.A. Jacobs, M. Tielen, J.B. Uytterhoeven, J. Catal. 50 (1977) 98.
[22] H. Feuer, J. Hooz, The Chemistry of the Ether Linkage, Wiley, New York, 1967, pp. 445–498.
[23] B.C. Gates, W. Rodriguez, J. Catal. 31 (1973) 27.
[24] R. Thornton, B.C. Gates, J. Catal. 34 (1974) 275.
[25] J.A. Ballantine, M. Davies, I. Patel, J.H. Purnell, M. Rayanakorn, K.J. Williams, J.M. Thomas, J. Mol. Catal. 26 (1984) 37.
[26] R.G. Greenler, J. Chem. Phys. 37 (1962) 2094.
[27] R.O. Kagel, J. Chem. Phys. 71 (1967) 844.
[28] L. Lietti, Q. Sun, R.G. Herman, K. Klier, Catal. Today 27 (1996) 151.
[29] G. Larsen, L.M. Petkovic, Appl. Catal. A: Gen. 148 (1996) 155.
[30] M.C. Cruz Costa, L.F. Hodson, A.W. Johnstone, J.Y. Liu, D. Whittaker, J. Mol. Catal. A: Chem. 142 (1999) 349.
[31] M.A. Harmer, W.E. Farneth, Q. Sun, J. Am. Chem. Soc. 118 (1996) 7708.
[32] D. Farcasiu, A. Ghenciu, G. Marino, K.D. Rose, J. Am. Chem. Soc. 119 (1997) 11826.
[33] A. Heidekum, M.A. Harmer, W.F. Holderich, J. Catal. 181 (1999) 217.
[34] A. Heidekum, M.A. Harmer, W.F. Holderich, J. Catal. 188 (1999) 230.
[35] M.A. Makarova, C. Williams, V.N. Romannikov, K.I. Zamaraev, J.M. Thomas, J. Chem. Soc., Faraday Trans. 86 (1990) 581.
[36] M.A. Makarova, C. Williams, K.I. Zamaraev, J.M. Thomas, J. Chem. Soc., Faraday Trans. 90 (1994) 2147.
[37] R.A. Sheldon, J.A. Elings, S.K. Lee, H.E.B. Lempers, R.S. Downing, J. Mol. Catal. A: Chem. 134 (1998) 129.
[38] D. Barthomeuf, Catal. Rev. 38 (1996) 521.
[39] B. Coughlan, M.A. Keane, J. Catal. 123 (1990) 364.
[40] B. Coughlan, M.A. Keane, J. Colloid. Interf. Sci. 137 (1990) 483.
[41] M.A. Keane, Microporous Mater. 3 (1994) 93.
[42] P.P. Lai, L.V.C. Rees, J. Chem. Soc., Faraday Trans. I 72 (1976) 1840.
[43] S.R. Samms, S. Wasmus, J. Savinell, J. Electrochem. Soc. 143 (1996) 1498.
[44] H. Kosslick, H. Landmesser, R. Fricke, J. Chem. Soc., Faraday Trans. 93 (1997) 1849.
[45] A. Auroux, Topic Catal. 4 (1997) 71.
[46] A. Auroux, M. Muscas, D.J. Coster, J.J. Fricke, Catal. Lett. 28 (1994) 179.
[47] B.E. Spiekwak, B.E. Handy, S.B. Sharma, J.A. Dumesic, Catal. Lett. 23 (1994) 207.
[48] B. Coughlan, M.A. Keane, Catal. Lett. 5 (1990) 113.
[49] F. Arena, F. Frusteri, A. Parmaliana, Appl. Catal. A: Gen. 187 (1999) 127.
[50] J.L. Falconer, J.A. Schwarz, Catal. Rev.-Sci. Eng. 25 (1983) 141.

[51] R.J. Behm, G. Ertl, V. Penka, Surf. Sci. 160 (1985) 387.

[52] N. Vasquez, A. Muscat, R.J. Madix, Surf. Sci. 301 (1994) 83.

[53] J.L. Gland, R.J. Madix, R.W. McCabe, C. DeMaggio, Surf. Sci. 143 (1984) 46.

[54] G.D. Weatherbee, C.H. Bartholomew, J. Catal. 87 (1984) 55.

[55] X.-Z. Jiang, S.A. Stevenson, J.A. Dumesic, J. Catal. 91 (1985) 11.

[56] Y.H. Hu, E. Ruckenstein, J. Catal. 163 (1996) 306.

[57] S.G. Lias, J.F. Liebman, R.D. Levin, S.A. Kafafi, NIST Standard Reference Database 25, Structure and Properties, Version 2.01, 1994.

[58] W.H. Brown, Organic Chemistry, Saunders, New York, 1995.

[59] P.A. Jacobs, J.B. Uytterhoeven, J. Catal. 50 (1977) 109.

[60] H.L. Del Castillo, P. Grange, Appl. Catal. A: Gen. 103 (1993) 23.

[61] M. Guisnet, P. Magnoux, in: B. Delmon, G.F. Froment (Eds.), Catalyst Deactivation, Elsevier, Amsterdam, 1994, p. 53.

[62] M.R. Guisnet, Acc. Res. Chem. 23 (1990) 392.

[63] E.A. Lombardo, G.A. Sill, W.K. Hall, J. Catal. 22 (1971) 54.

[64] Q. Sun, M.A. Harmer, W.E. Farneth, Chem. Commun. (1996) 1201.

[65] F. Kooli, W. Jones, J. Mater. Chem. 8 (1998) 2119.

[66] F. Kooli, J. Bovey, W. Jones, J. Mater. Chem. 1 (1997) 153.

[67] D. Chatterjee, H.M. Mody, K.N. Bhatt, J. Mol. Catal. A: Chem. 104 (1995) 115.

[68] F.A. Carey, Organic Chemistry, McGraw-Hill, New York, 1987.

[69] C. Park, R.T.K. Baker, J. Catal. 179 (1998) 361.

[70] G. Larsen, E. Lotero, M. Nabity, L. Petkovic, C.A. Querini, in: C.H. Bartholomew, G.A. Fuentes (Eds.), Catalyst Deactivation, Elsevier, Amsterdam, 1997, p. 147.

[71] B. Coughlan, M.A. Keane, J. Catal. 138 (1992) 164.

[72] P.J.R. Chutoransky, W.L. Kranich, J. Catal. 21 (1977) 1.

[73] M.F. Guilleux, D. Delafosse, G.A. Martin, J.A. Dalmon, J. Chem. Soc., Faraday Trans. I 175 (1979) 165.

[74] Y. Gauthier, R. Baudoing-Savois, K. Heinz, H. Landskron, Surf. Sci. 251 (1991) 493.

[75] J.H. Onuferko, D.P. Woodruff, B.W. Holland, Surf. Sci. 87 (1979) 357.

[76] P. Gallezot, Y. Ben Taarit, B. Imelik, J. Catal. 26 (1972) 295.